Supporting information

Electrochemical Fabrication of Long-Range Ordered Macro-Microporous Metal-Organic Framework Films

Sijia Qin, Sai Zhang, Min Chen*, and Limin Wu*

Department of Materials Science, State Key Laboratory of Molecular Engineering of Polymers, Fudan University, Shanghai, 200433, China

*E-mail: chenmin@fudan.edu.cn, lmw@fudan.edu.cn

Experimental Section

Here, we prepared three-dimensional ordered macro-microporous metal-organic frameworks (3DOM-ZIF-8) film on planar conducting supports like FTO.

Materials and characterization

Commercially available chemicals were used as purchased without further purification. Zinc acetate dehydrate ($Zn(Ac)_2$, AR, 99%, Aladdin), 2-Methylimidazole (98%, Aladdin), methanol (Shanghai Dahe Co. Ltd). The standardized PS latex particles (200, 250, 300, 350 and 400 nm) were obtained from the Shanghai Hugebio Technology Company. All chemicals used for the vapor sensing experiments are reagent grade and were purchased from Aladdin.

The morphology of the PS colloidal crystal templates and the ordered 3DOM ZIF-8 films were characterized using FE-SEM (Philips XL 30) at an accelerating voltage of 3 kV. The skeleton of ZIF-8 was examined using X-ray diffraction (Bruker Focus D8 diffractometer) with CuKα radiation (40 kV, λ = 1.5406 Å), Ultraviolet-visible absorption spectra were recorded on a Lambda 35 (Perkin-Elmer) UV-vis spectrophotometer. Raman spectrum was recorded using XPloRA (HORIBA JobinYvon) instrument with 520 nm Ar ion laser. Oxygen plasma (CPC-B-13.56, CIF (Beijing) Tech Co., Ltd) was taken to make the surface hydrophilic. Tapping-mode atomic force microscopy (AFM, fast scan A61-1) images were conducted to identify the surface structure. When measuring AFM, the scanning rate is 0.1 Hz. XPS analysis were measured by Thermo Scientific K-Alpha from Shiyanjia Lab (www.shiyanjia.com). Nitrogen adsorption-desorption isotherms were measured by micromeritics ASAP 2460 from Shiyanjia Lab. BET method was used to calculate the surface areas. Electrophoretic deposition was carried out on electrochemical workstation (CHI660E). A digital camera (X-T20, Fujifilm) was used to capture the digital photographs with a white LED light source. Reflectance measurements were recorded with the same instrument (R1, angle-resolved spectrum system, ideaoptics,

China) using halogen lamp. Optical measurements with all samples were performed in reflectance mode.

All data processing and presentation, including the data of measured reflectance spectra and the principal component analysis, were conducted using OriginLab OriginPro 2021 software. There is an application in OriginPro 2021 called "PCASpec", which performs principal component analysis for spectroscopy data. The website is:

https://www.originlab.com/fileExchange/details.aspx?fid=326

Preparation of opal-structure PS template

The preparation of the opal-structure PS template was carried out by first ultrasonically washing the fluorine-doped tin oxide (FTO) substrates ($7 \Omega/cm^2$, $1 \times 2 cm^2$) in acetone, ethanol, and DI water. After drying under a nitrogen flow, the FTO substrates were subjected to an oxygen plasma treatment for 2 min to make the surface hydrophilic. A vertical deposition technique was then employed for the fabrication of fully dense FCC colloidal crystal films on FTO glass. Each hydrophilic FTO substrate was submerged vertically into the prepared PS colloidal suspension (0.1 %), and the entire setup was kept at 65 °C until the complete volatilization of water. Next, the stability of the resulting spheres was resulting enhanced by sintering at 90 °C for 2 h.

Fabrication of 3DOM ZIF-8 film

The synthesis of 3DOM ZIF-8 inverse-opal-structure was performed by first dissolving a solid mixture of 2-methylimidazole (0.205 g) and zinc acetate dihydrate (0.1375 g) in 50 mL methanol followed by stirring to dissolve all chemicals. The molar ratio of ligand to metal was set to 4:1, and FTO glass with PS coating was immersed in the above-prepared solution. A constant current ($-0.7 mA/cm^2$) was applied for 200 s at room temperature to generate the ZIF-8 film. Note that the solution required stirring at 600 rpm to promote mass transfer during

3

the electrodeposition. After deposition, PS particles were removed by soaking in tetrahydrofuran (THF) for 3 h followed by treating with ultrasounds to yield the inverse-opal structure.

**Rapid growth of ZIF-8 nanoparticles at room temperature**

The growth was carried out by first preparing 50 mL methanol solution of $Zn(Ac)_2$ (0.1375 g) and of 2-methylimidazole (0.205 g) was prepared. After complete dissolution, $Zn(Ac)_2$ was quickly poured into 2-methylimidazole methanol solution and the mixture was stirred and collected by centrifugation followed by washing with methanol for three times and drying at room temperature.

To examine the selective chemical response of the photonic structure, a 1×1 cm^2 region of the 3DOM inverse opal film was exposed to various alcohol homologs vapors. The diameter of the illumination spot of the fiber optic was around 5 mm.

Principal components analysis

PCA is used for classification of multivariate data. PCA reduces a multidimensional data set for its easier interpretation by calculating orthogonal principal components that are oriented in the direction of the maximum variance within the data set. The eigenvectors of the data matrix are called principal components and they are uncorrelated among them. The first principal component contains the highest degree of variance, and other PCs follow in the order of decreasing variance. Thus, PCA concentrates the most significant characteristic of the data into a lower dimensional space. During data analysis, more than 800 data points of each differential reflectance spectrum (from 400 to 800 nm) were used for the classification algorithms.
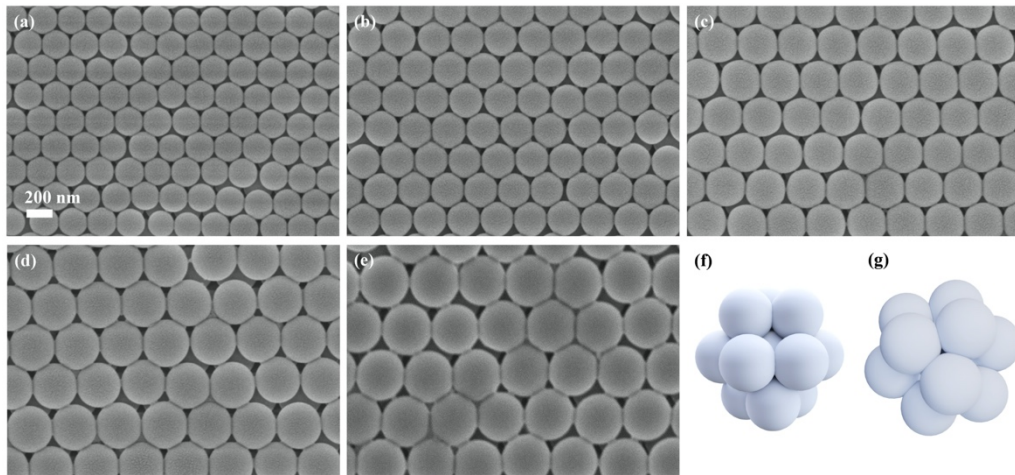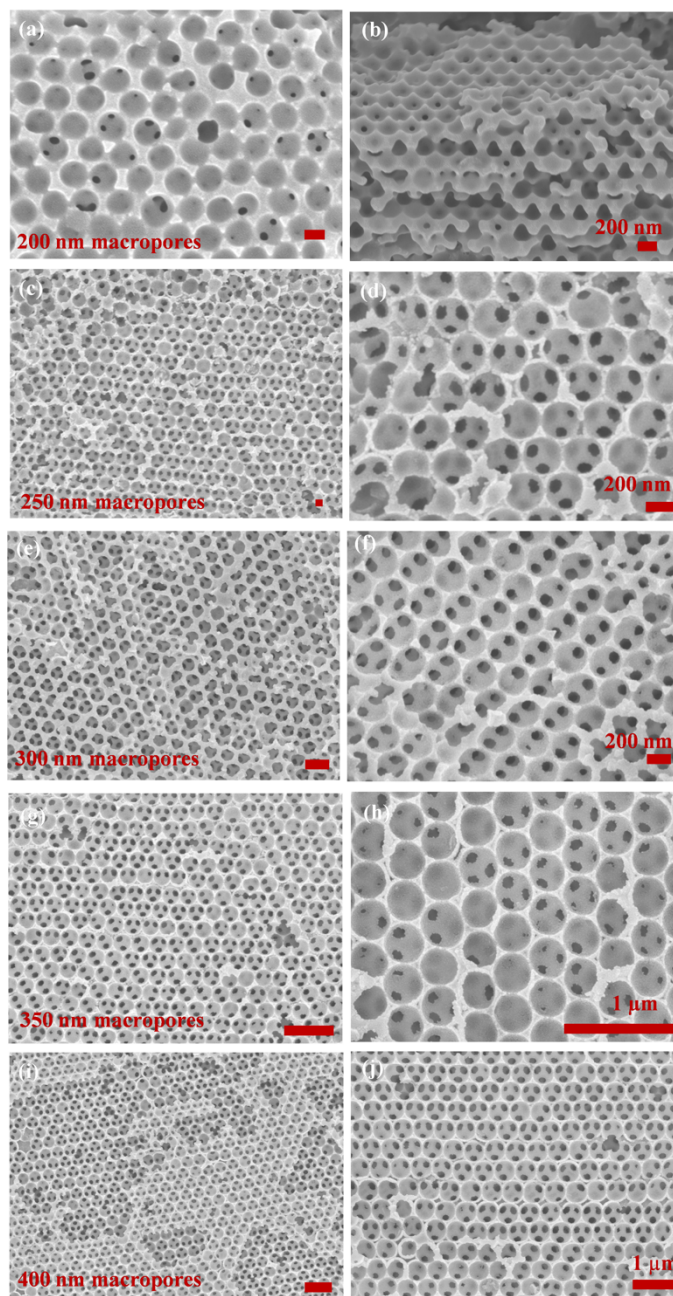
Fig. S1. The hard template PS uniformed microspheres with diameters of (a) 200 nm, (b) 250 nm, (c) 300 nm, (d) 350 nm, and (e) 400 nm. The water evaporation drives polystyrene spheres to assembly in FCC lattices on the FTO substrate. (f) and (g) Models of the hexagonally arranged PS spheres.
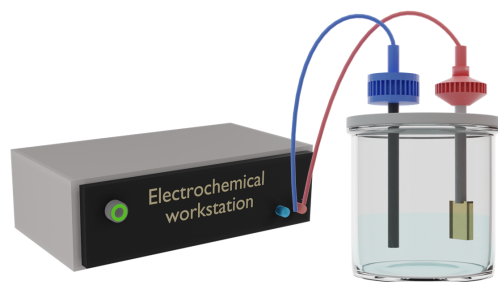
Fig. S2. The electrochemical cell used for the cathodic electrodeposition.

Fig. S3. SEM image of various 3DOM ZIF-8 films with macropore sizes of 200 to 400 nm determined by carefully controlling the diameter of PS templates: (a-b) 200 nm, (c-d) 250 nm, (e-f) 300 nm, (g-h) 350 nm, and (i-j) 400 nm. Some inverted cracks in the film are transferred from the host opal template.
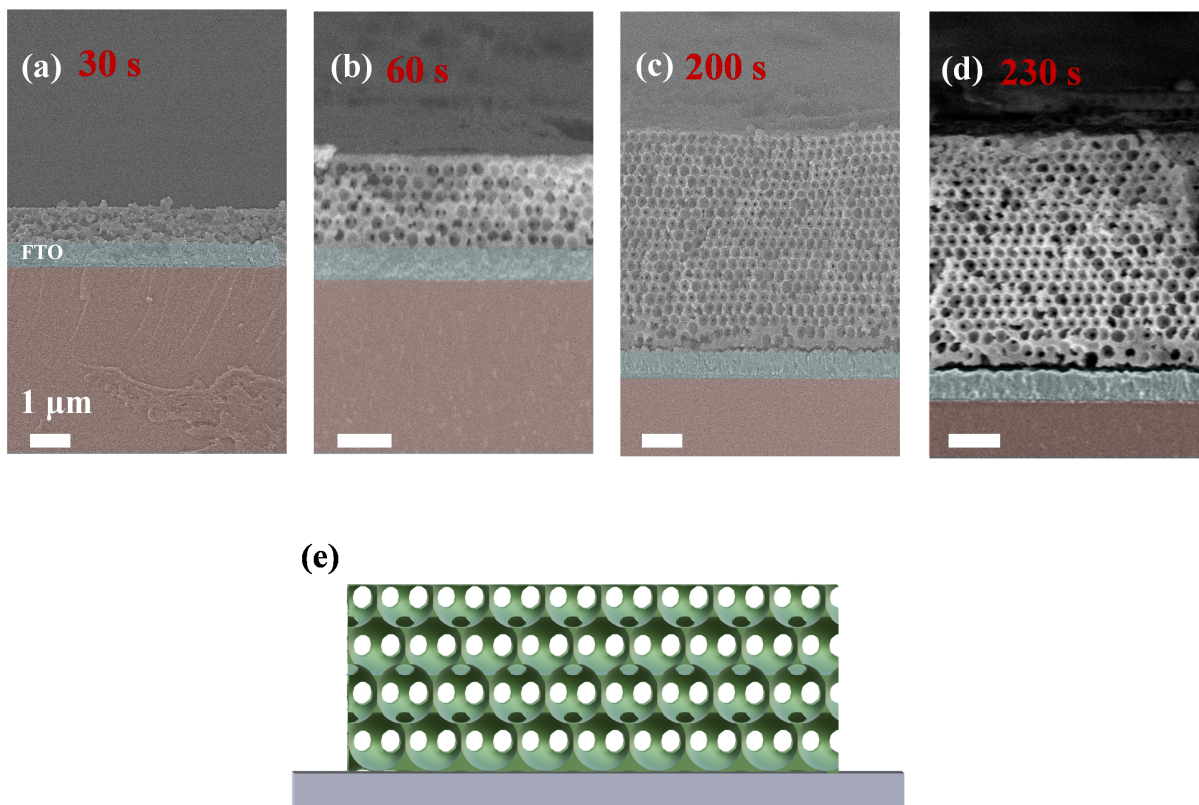
Fig. S4. Cross-sectional of 3DOM ZIF-8 formation on the FTO was recorded for different time (a) 30 s, (b) 60 s, and (c) 200 s, and (d) 230 s, respectively. It is observed that the film has reached the upper limit of the thickness even with longer time (more than 200 s). (e) illustration of 3DOM ZIF-8 film on FTO substrate obtained by the cathodic electrodeposition method.
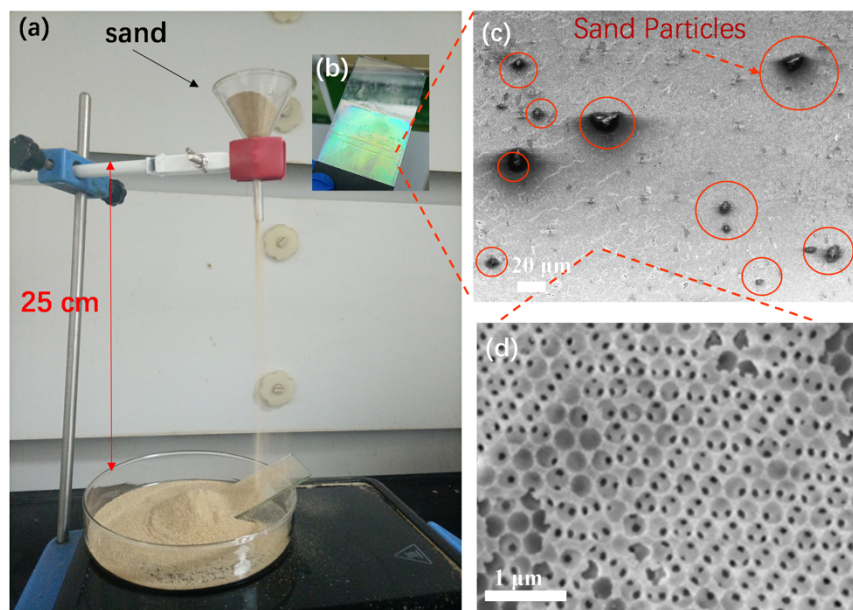
Fig. S5. (a) Stability of 3DOM ZIF-8 by sand abrasive test driven by gravity (20 g sand). (b) Photograph of this film treated with sand. (c) The SEM image of 3DOM ZIF-8 film at low magnification. It is observed that film is still intact and there is some residual sand on the surface. (d) The structure of 3DOM ZIF-8 film.
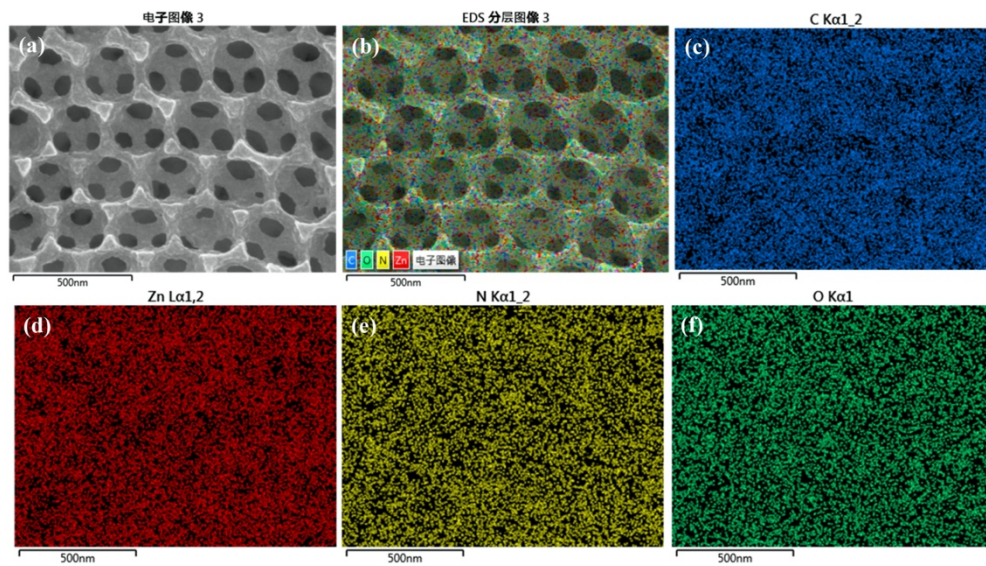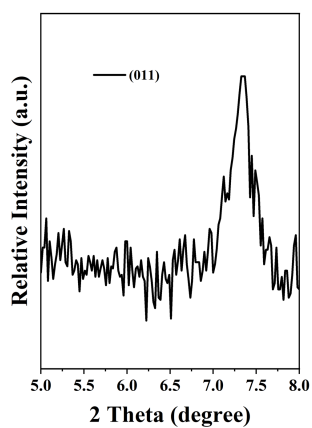
Fig. S6. EDS element mappings of the film 300 nm, reflecting homogeneously distributed C, Zn, N and O elements in the structure.
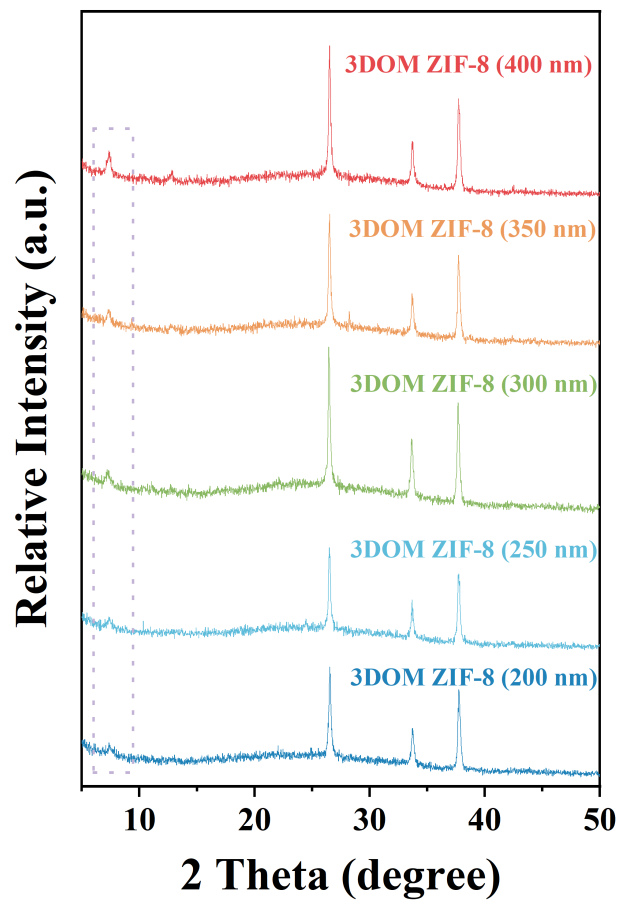
Fig. S7. XRD patterns of 3DOM ZIF-8 film with different macropores. From bottom to top: 200, 250, 300, 350, and 400 nm.
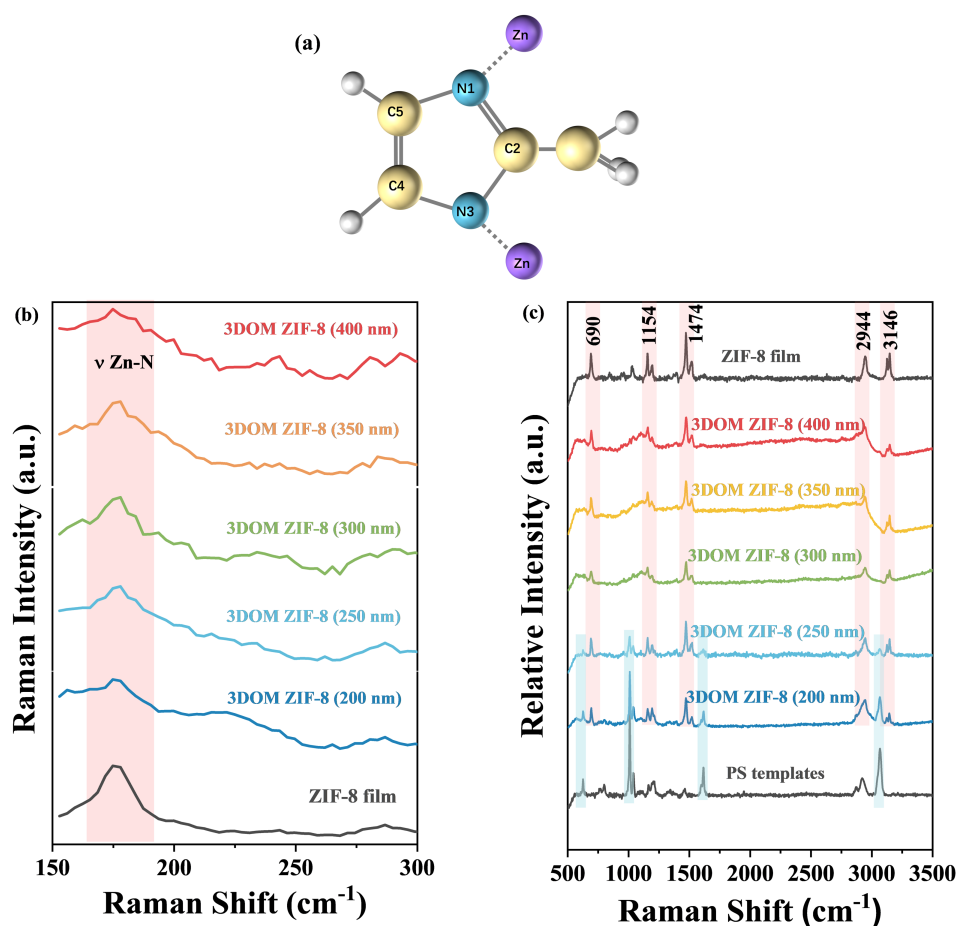
Fig. S8. XRD pattern of 3DOM inverse opal ZIF-8 film at (011) peak. The average particle sizes

are calculated from the strongest diffraction (011) by the Scherrer equation.[1]

$$D = \frac{K\lambda}{B\cos\theta}$$

According to the formula, the average crystalline size of the ZIF-8 is in the 23.6 nm scale.

Fig. S9. Raman spectra of 3DOM ZIF-8 electrodeposited film on FTO and ZIF-8 powder. The bands around 170 cm^{-1} are attributed to Zn-N stretching. Characteristic bands are observed at 690 cm^{-1} (imidazole ring puckering), 1154 cm^{-1} (C5-N stretching), 1474 cm^{-1} (methyl bending), 2944 cm^{-1} (C-H stretching of methyl), and 3146 cm^{-1} (C-H stretching of aromatic) respectively. Limited by small pore size, some residual PS from exist in macropores with 200 and 250 nm in size, leading to typical PS peaks in the spectra. Together, these results show the successful synthesis of 3DOM ZIF-8 film with different macropore sizes.

13
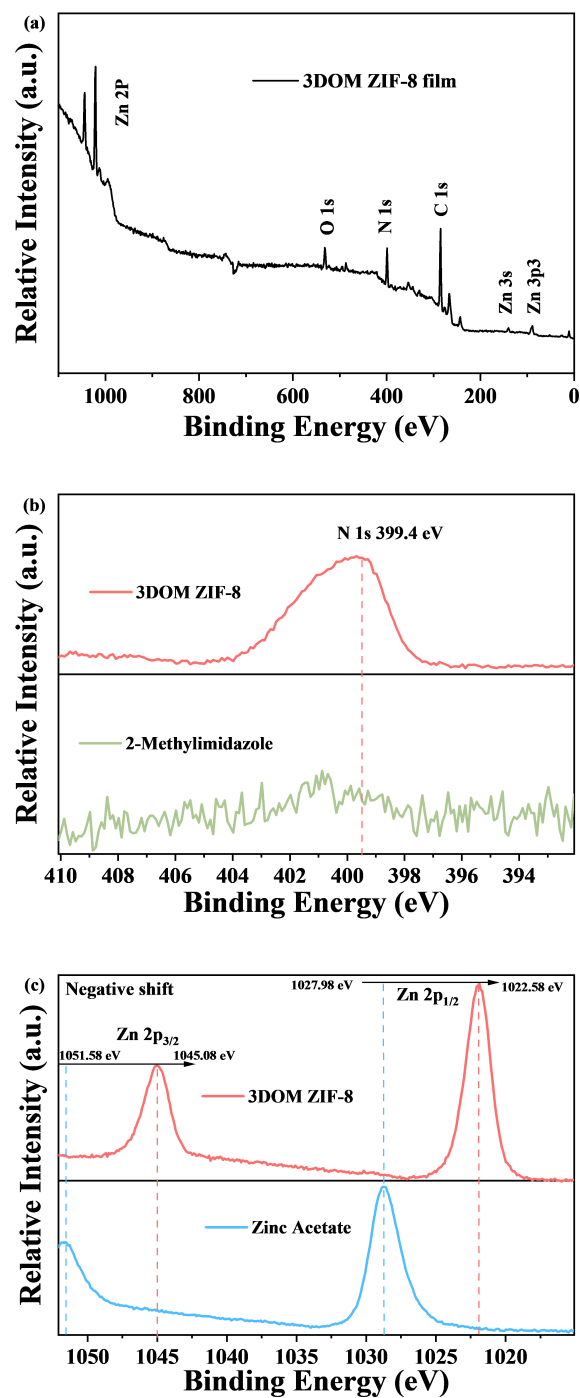
Fig. S10. The XPS survey spectra of (a) integrated XPS spectrum of 3DOM ZIF-8 inverse opal film. (b, c) Zn 2p and (e, d) N 1s XPS spectra of 2-methylimidazole and 3DOM inverse opal film, respectively.
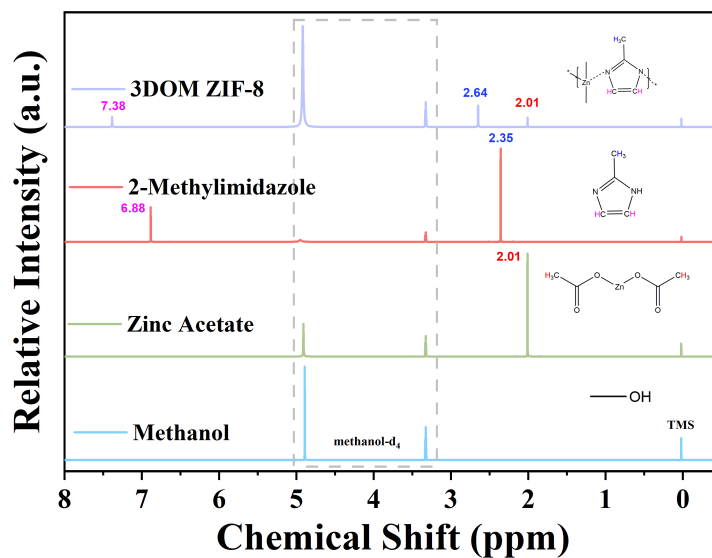
Fig. S11. ^{1}H NMR spectra of zinc acetate, 2-methylimidazole, and mixed precursors (electrodeposition ZIF-8) in methanol-d4. Shifts in peaks of 3DOM ZIF-8 are observed and can be attributed to the complexation of Zn ions and ligand 2-methylimidazole.
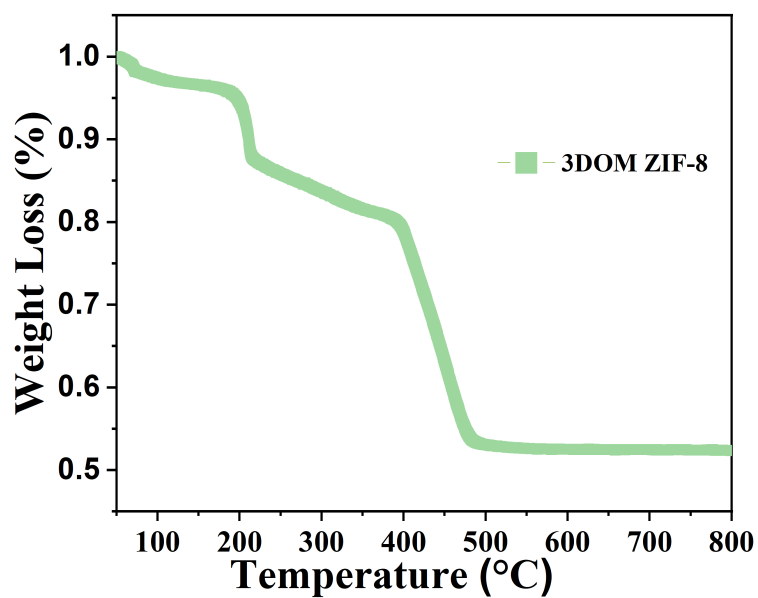
Fig. S12. TG profiles of film samples (Heating rate 10 °C min^{-1}, nitrogen atmosphere). Two weight changes exist at temperatures of 50 – 800 °C, and attributed to evaporation of physically adsorbed water (200 °C) followed by decomposition of ligand in the composite (400 °C) and simultaneous collapse of the framework.
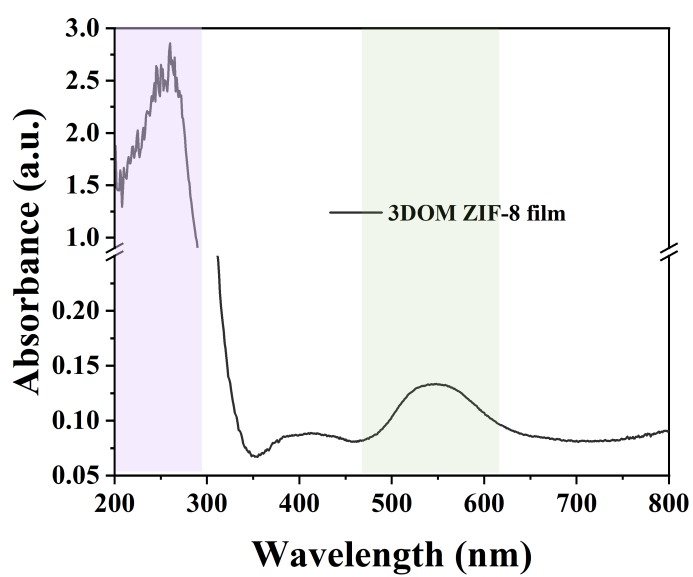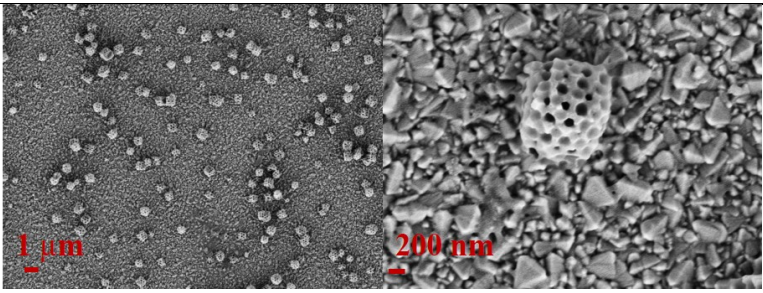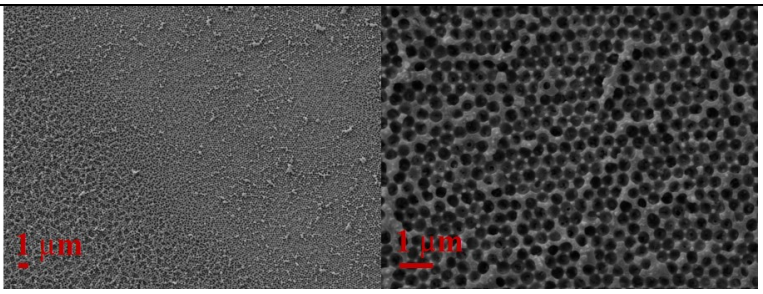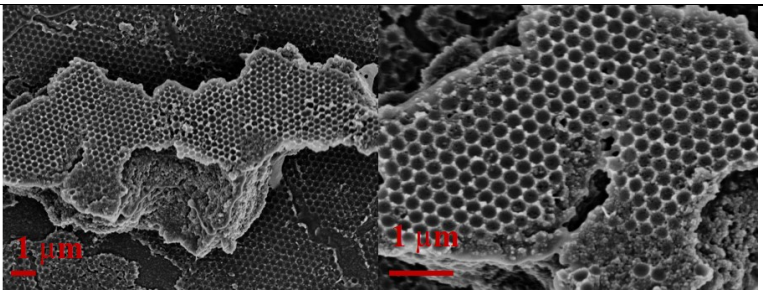
Fig. S13. UV spectra of 3DOM ZIF-8 film. There is a typical absorption peak around 540 nm

owing to the ordered inverse-opal structure.
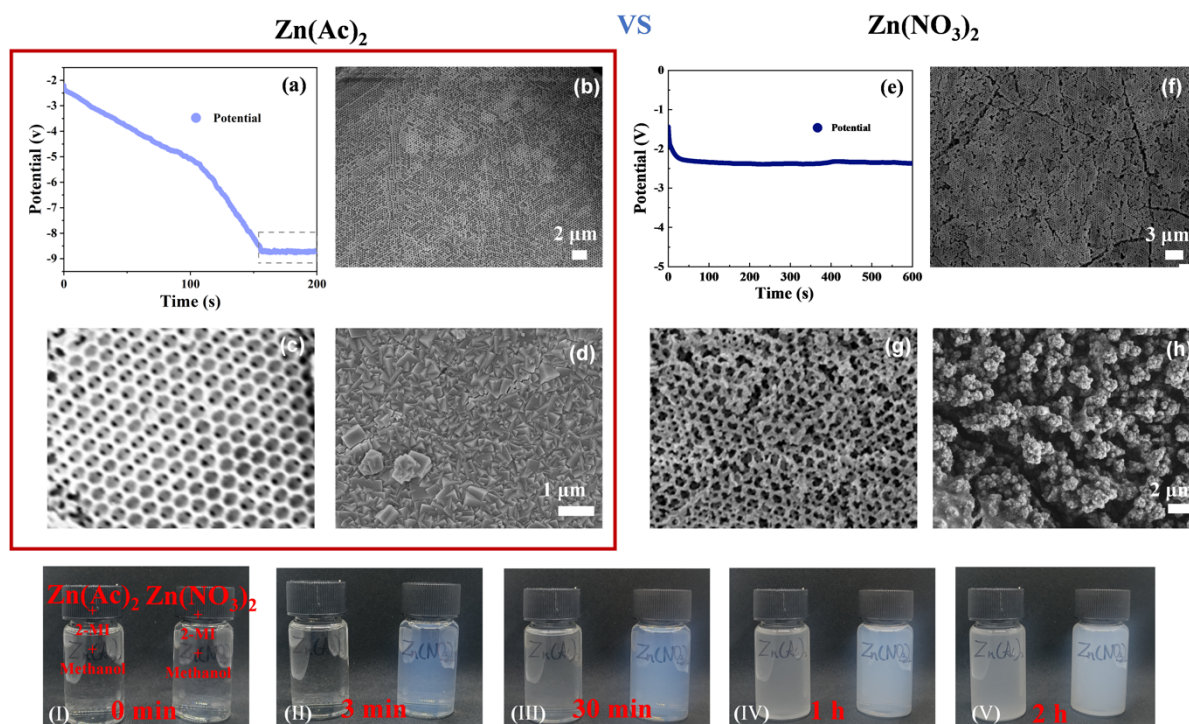
Fig. S14. A comparison of the zinc acetates for fabricating 3DOM ZIF-8 films with conventional zinc nitrate. (a, e) The change of potential during the cathodic electrochemical deposition; (b, f) the resulting 3DOM ZIF-8 films at low magnification; (c, g) the 3DOM ZIF-8 films in high resolution; (d, h) the ZIF-8 films without PS templates. The metal source was (a-d) zinc acetate, (e-h) zinc nitrate. Zinc acetate could act as "modulator" to the regulate reaction rate, so that high-qualified 3DOM ZIF-8 films are obtained. In contrast, crystallization rate in zinc nitrate and 2-methylimidazole solution was too fast to be well controlled in the electric filed to prepare continuous 3DOM ZIF-8 films. (I-V) The influence of metal precursor on the spontaneous synthesis of the ZIF-8 when using the same molar ratio of metal/ligand in methanol. This controlled experiment proved that the crystallization rate between zinc nitrate and 2-methylimidazole was much faster than zinc acetate and 2-methylimidazole (the solution of zinc nitrate has become turbid within 3 min).
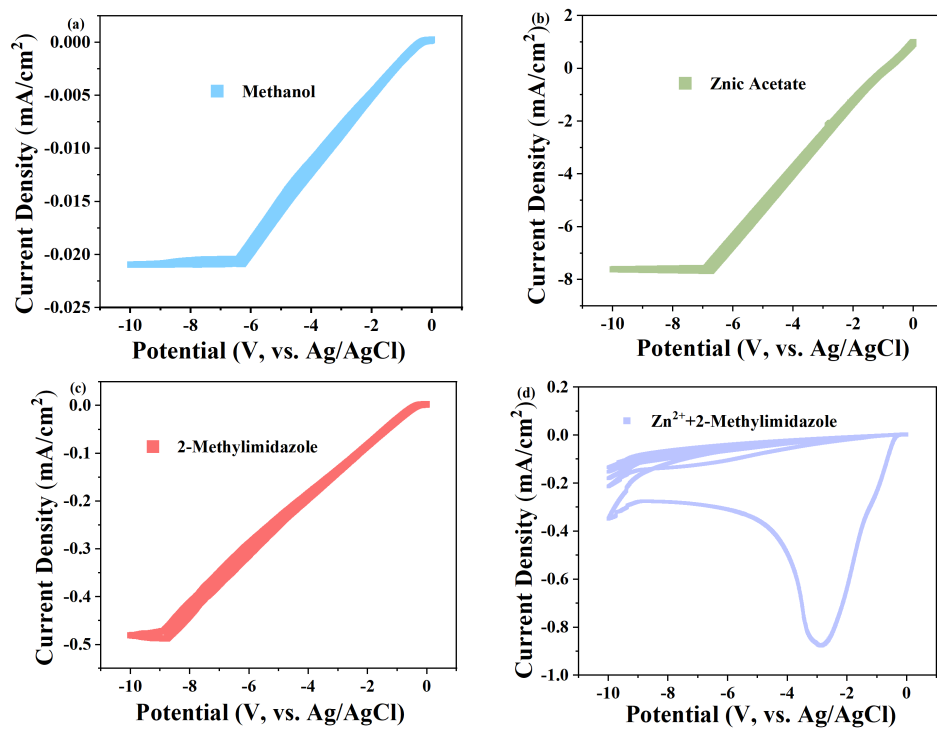
Fig. S15. Cyclic voltammetry curve (CV) of: (a) pure methanol, (b) zinc acetate aqueous solutions, (c) 2-methylimidazole aqueous solution, and (d) 3DOM inverse opal ZIF-8 film synthesis precursor.

	Conditions	Morphology
A	Pulse electrodeposition method, 100 ms on and 300 ms off, and 80 k cycles.	
B	The ratio of precursor metal to the ligand is 1:2.	
C	Infiltration of the precursors into the PS arrays by the conventional method.	

Fig. S16. (A) The pulse electrodeposition is also used to prepare the 3DOM ZIF-8 film. However, tiny solid ZIF-8 nanocrystals with macro-microporous are obtained under these conditions. (B) Various applied constant potential, and different metal/ligand ratios are examined. Under these conditions, only monolayered ZIF-8 with macropores is obtained. In addition, the film is not continuous. (C) Deprotonation agents (sodium formate, $NH_3 \cdot H_2O$, and triethylamine) can enhance heterogeneous nucleation and promote the intergrowth of ZIF-8 crystals in conventional ZIF-8 film synthesis. Infiltrating the precursors into the PS array is a classic method to acquire inverse opal. To this end, different deprotonation agents are mixed with the precursor's solutions followed by filling the PS arrays. However, only brittle crystals are obtained owing to the energetic barrier and rapid crystallization.
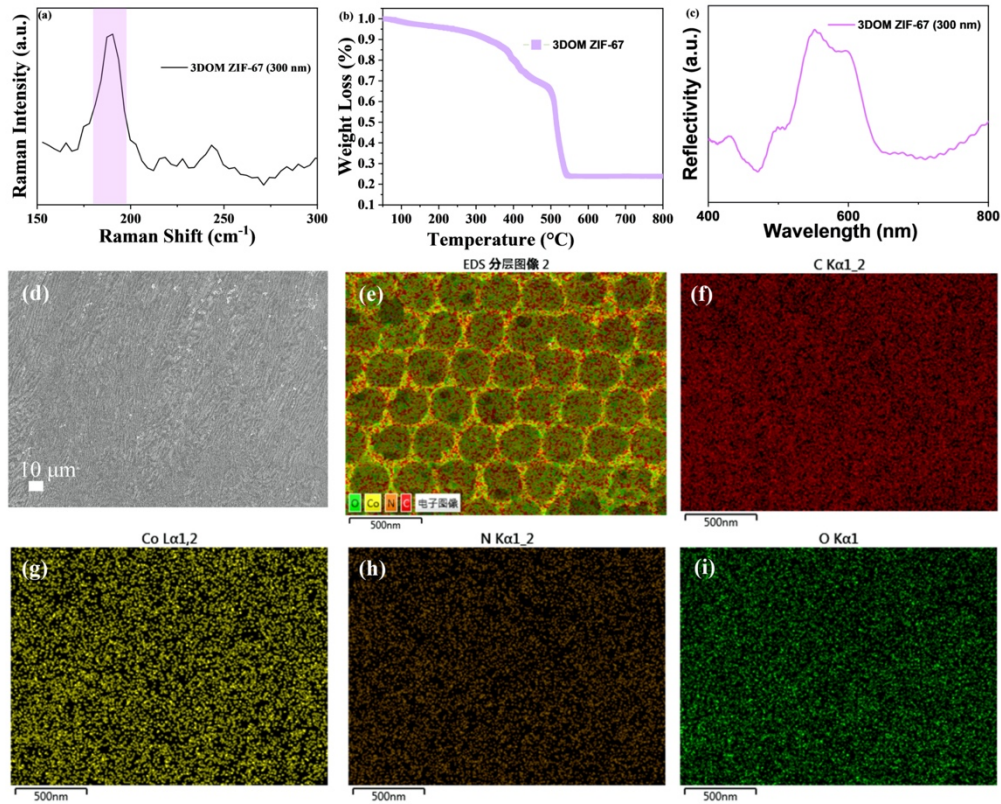
Fig. S17. (a) XRD spectra of 3DOM ZIF-67 film in comparison with the simulated pattern of sodalite structure. (b) TG spectra and (c) reflectance spectra. The 3DOM ZIF-67 inverse opal film is shown in green-purple due to the combined of the structural color and the natural color of the ZIF-67. (d-i) EDS mapping of the 3DOM ZIF-67 film.
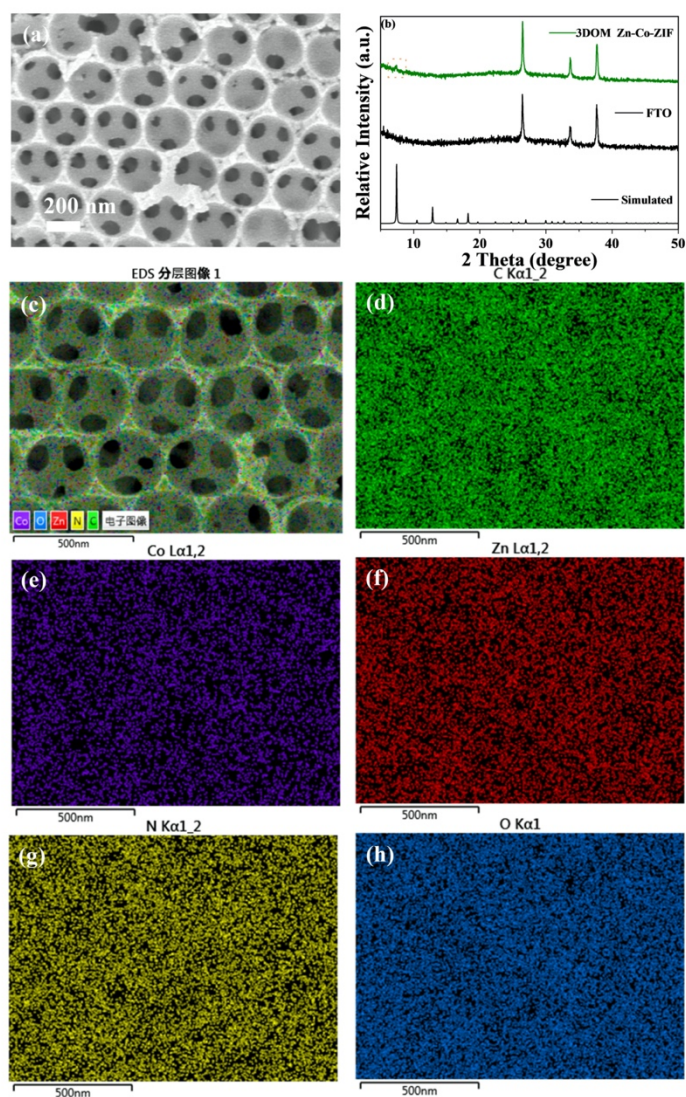
Fig. S18. (a) SEM and (b) XRD spectra of 3DOM Zn/Co-ZIF film in comparison with the simulated pattern. (c-h) EDS mapping of the film. Zn and Co are simultaneously incorporated into the framework, resulting in 3DOM Zn/Co-ZIF inverse opal film. According to the literature, the metals' location in the crystal structure of Zn/Co-ZIF is completely random.[2]
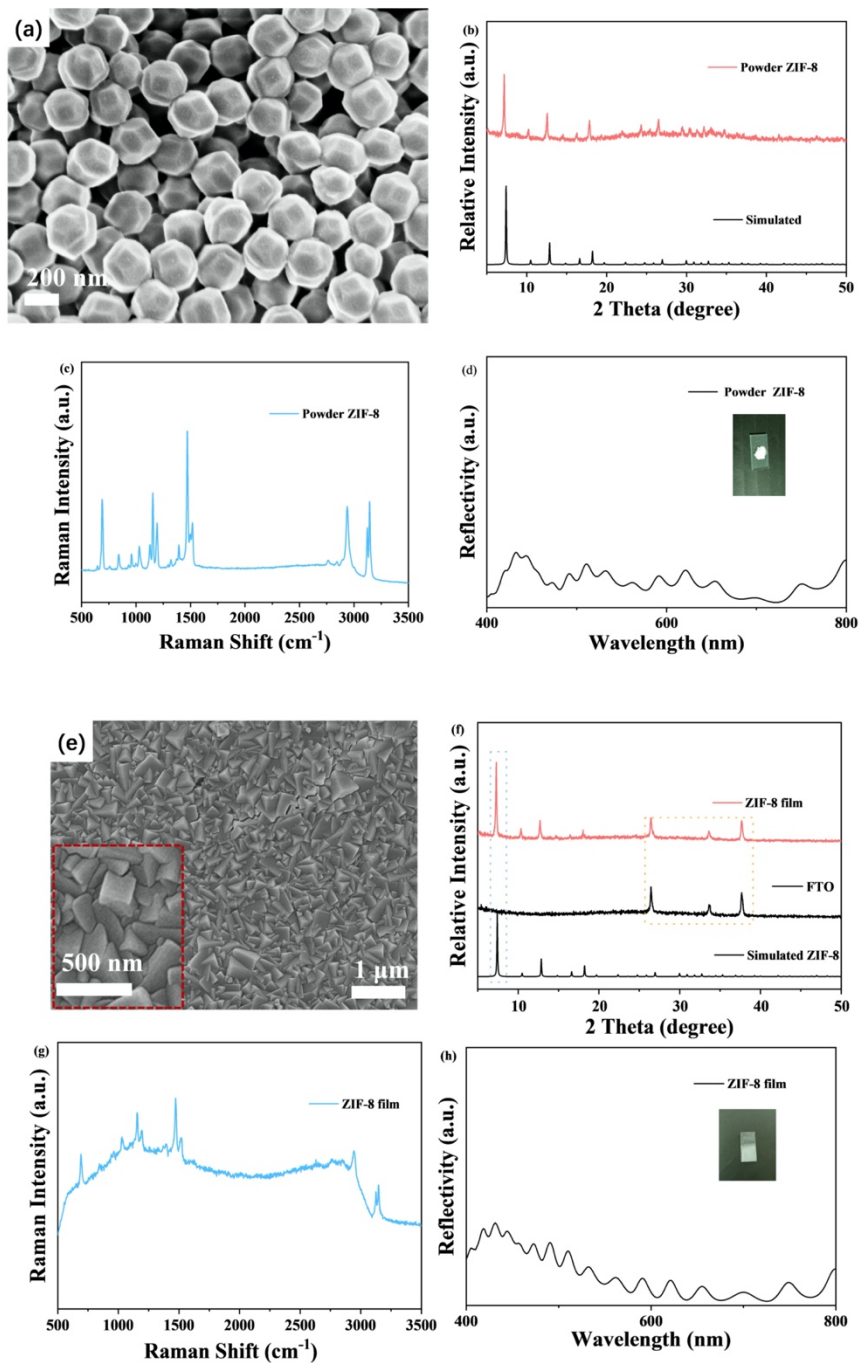
Fig. S19. The powder ZIF-8 deposited on FTO substrates (a) SEM pattern, (b) XRD spectra, (c) Raman spectra, and (d) reflectance spectroscopy. ZIF-8 film without macropores (e) SEM pattern, (f) XRD spectra, (g) Raman spectra, and (h) reflectance spectroscopy. The powder ZIF-8 was randomly distributed on the substrate, leading to irregular peaks in the spectra. As for films without ordered macropores, only one broad shoulder appeared in the spectrum and the color of the films was white.
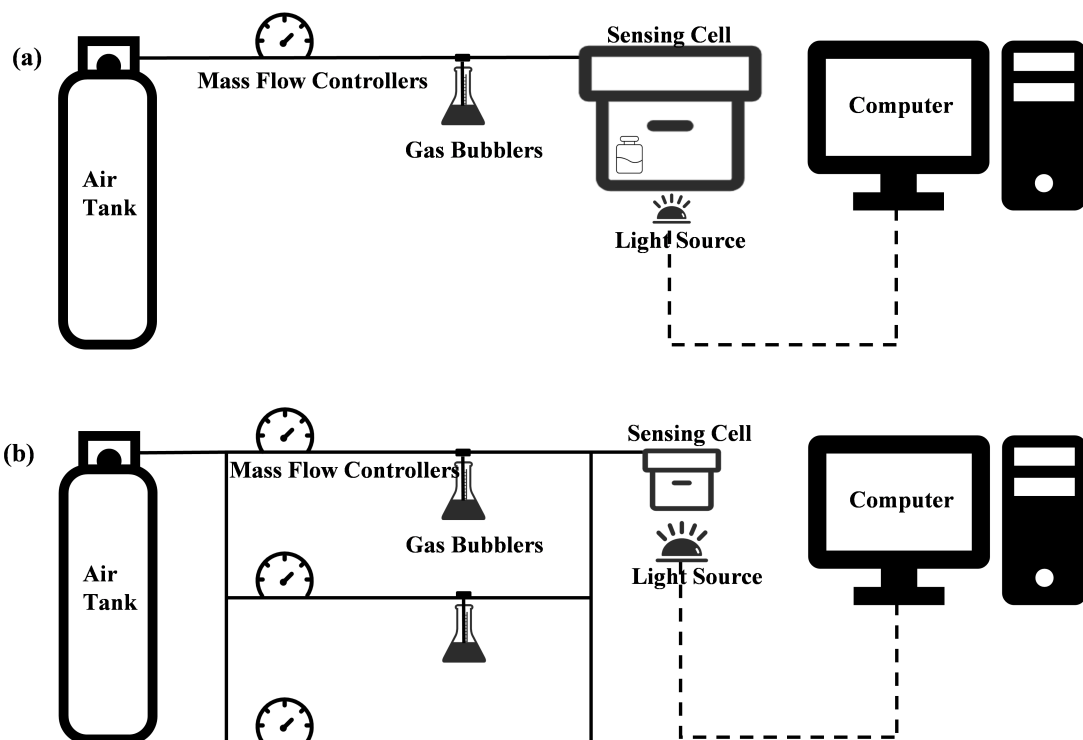
Fig. S20. Schematic diagram of gas-response of the fabricated 3DOM ZIF-8 inverse opal photonic film used in (a) single gas, and (b) mixed gas sensing tests. The fiber-optic port is designed to illuminate the sensing film.

24
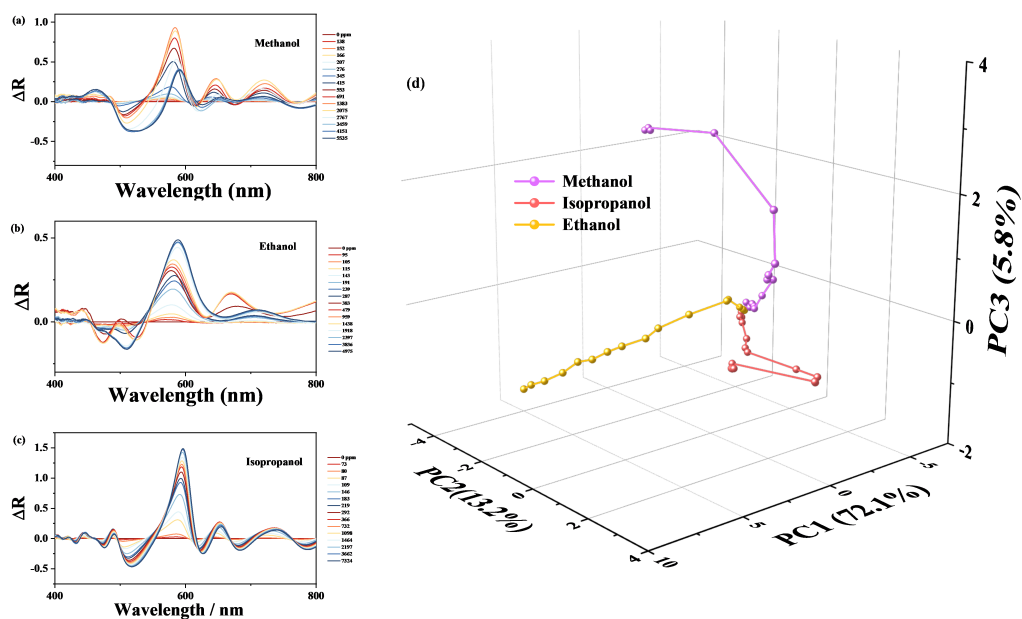
Fig. S21. Selective detection of vapors by ordered 3DOM ZIF-8 inverse opal film. Differential reflectance spectra of vapors (a) methanol, (b) ethanol, and (c) isopropanol. Vapor concentrations are shown in legend. (d) To differentiate these responses quantitatively, multivariate analysis is carried out using PCA tools by processing differential reflectance spectra over 400-800 nm range.
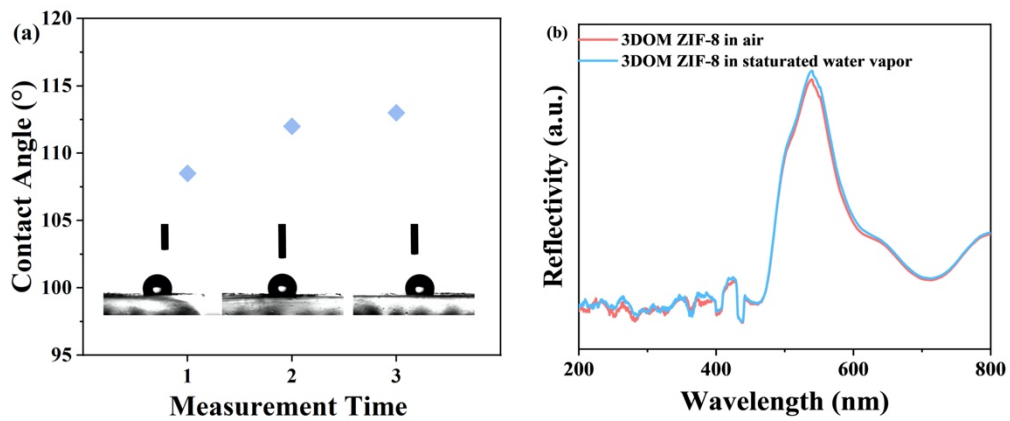
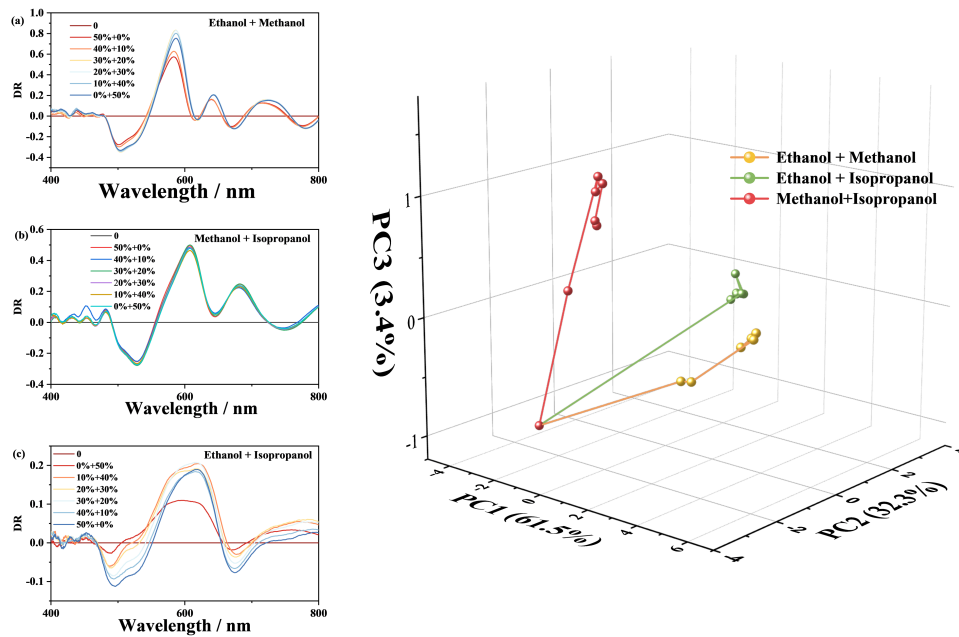**Fig. S22.** Water-drop profiles of 3DOM ZIF-8 films with 300 nm diameter macropores and corresponding contact angles (CA). The picture shows CA around 110°.
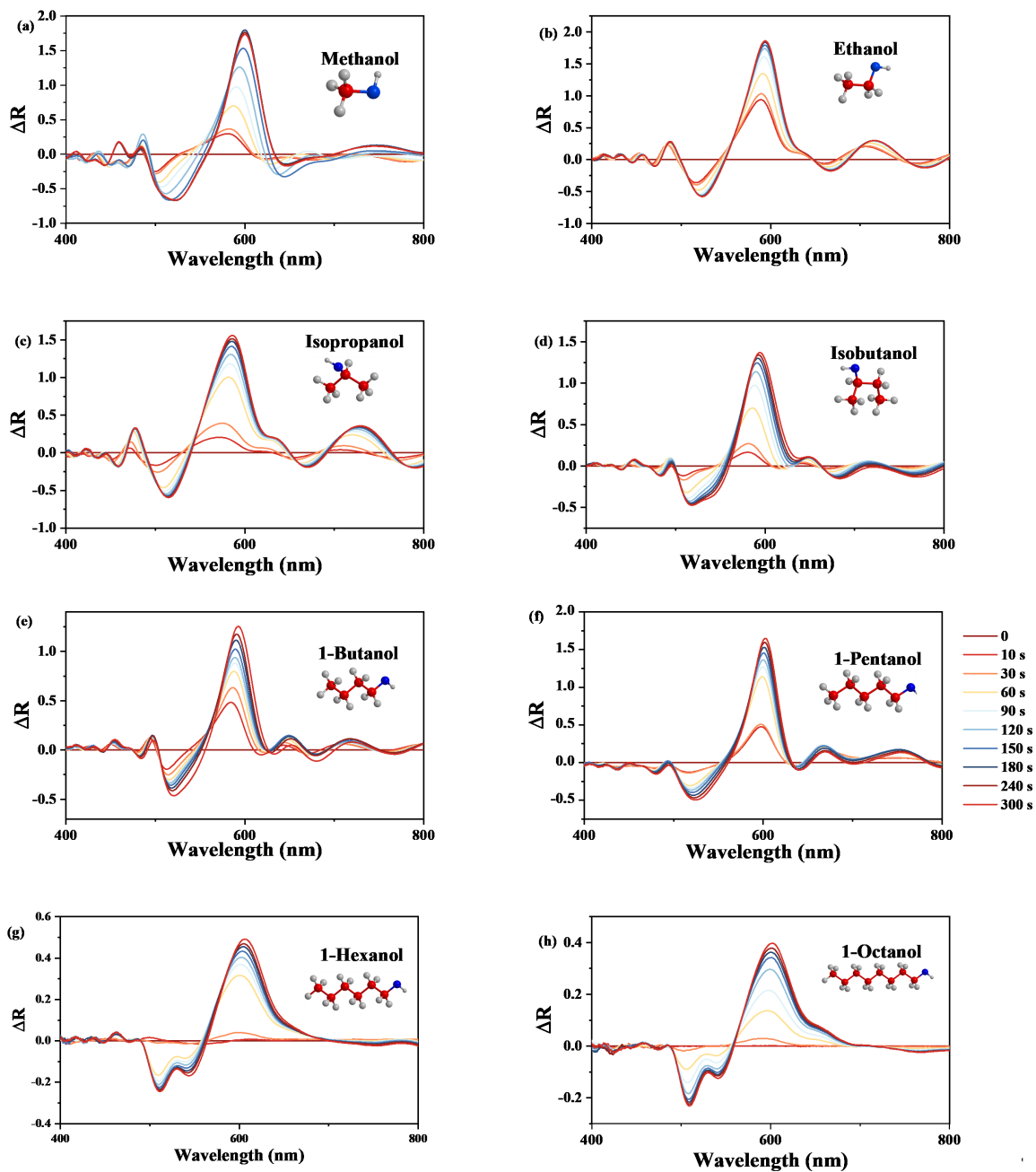
Fig. S23. Averaged differential reflectance spectra of (a) methanol, (b) ethanol, (c) isopropanol, (d) isobutanol, (e) 1-butanol, (f) 1-pentanol, (g) 1-hexanol, and (h) 1-octanol measured using a 3DOM ZIF-8 film as a function of time.

Fig. S24. Differential reflectance ΔR spectra and corresponding PCA plots of the fabricated photonic 3DOM ZIF-8 inverse opal film upon exposure to binary vapor mixtures: (a) (methanol + ethanol), (b) (ethanol + isopropanol), and (c) (methanol + isopropanol).
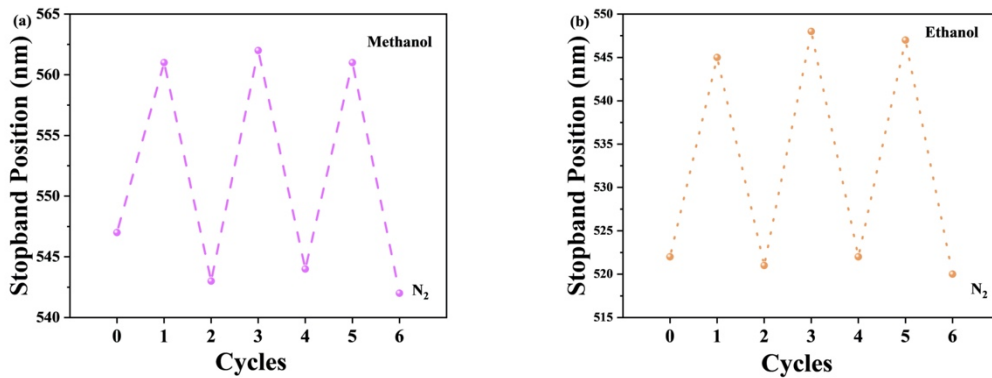
Fig. S25. Reversible changes of maximum stopband position for the 3DOM ZIF-8 film when alternately exposed to (a) methanol, (b) ethanol and nitrogen. The sensing of vapor was achieved by physical adsorption, so the peaks shifted towards longer wavelengths but fully recovered rapidly upon the introduction of pure nitrogen gas. Thanks to the hierarchical structures, the response was fast and stabilized after several seconds.

VOCs	Refractive index	Diameter (Å)
Methanol	1.3312	3.8
Ethanol	1.3616	4.18
Iso-propanol	1.3776	4.70
Iso-butanol	1.3959	5.40
1-butanol	1.399	-
1-pentanol	1.409	-
1-hexanol	1.4178	-
1-octanol	1.429	-

Table S1. Physical properties (diameter and refractive index) of linear alcohols homologs analytes tested in this study.

$$c = \frac{(\rho V / M)}{V_0 / (22.4L/mol)} = \frac{22.4\rho V}{MV_0} \times 10^6$$

Table S2. In this formula, c (ppm) refers to the concentration of the linear alcohols, ρ (g/mL) is the density of the alcohols, V (mL) represents the volume of the alcohols, M (g/mol) is the molecular weight, and V_0 (mL) denotes the volume of the gas chamber ($20 \times 10 \times 20$ mL).[3]

Materials	Method	Target Molecules	Concentrations	Analysis Method	References
HKUST-1, Cu(BTC), and Cu(BPDC) array	Quartz crystal microbalance	Volatile plant oils and their mixtures	1–40 mg/L	Principal component analysis. Linear discrimination analysis. Nearest neighbor analysis	61
ZIF-8, HKUST-1, and CAU-1-NH$_2$	Reflectance spectra	Methanol, Ethanol, 2-propanol, 1-hexanol	10%–100%	Principal component analysis.	60
HKUST-1, Cu(BDC), Cu(BPDC), Cu2(DCam)$_2$(dabco), Cu(DCam)$_2$(BiPy), and Cu$_2$(DCam)$_2$(BipyB) array	Quartz crystal microbalance	Aromatic plants	/	Principal component analysis. Linear discrimination analysis. Nearest neighbor analysis	62
ZIF-67-Co-Pd	Resistanee	Ethanol, Acetone	1-5 ppm	Principal component analysis.	63
3DOM ZIF-8 Film	Reflectance spectra	Linear alcohol homologs and their mixtures	138–5535ppm, 95–4975 ppm, 73–7324 ppm.	Principal component analysis.	This work

Table S3. Comparison of MOF-based sensors that have been used PCA.

Reference

[1]   S. H. Yu, Z. Chen, R. Wang, T. Ma, J. L. Wang, Y. Duan, Z. Z. Dai, J. Xu, H. J. Wang, J. Y. Yuan, H. L. Jiang, Y. W. Yin, X. G. Li, M. R. Gao, *Angew. Chem., Int. Ed.*, 2021, **60**, 14124-14130.

[2]   K. Zhou, B. Mousavi, Z. Luo, S. Phatanasri, S. Chaemchuen, F. Verpoort, *J. Mater. Chem. A*, 2017, **5**, 952-957.

[3]   X. Fan, B. Du, *Sens. Actuators, B* 2012, **166-167**, 753-760.